Journal of Molecular Structure 1374 (2026) 146840

Contents lists available at ScienceDirect

Journal of Molecular Structure

journal homepage: www.elsevier.com/locate/molstr

Lead(II) compounds with 2-acetylpyridine benzoylhydrazone: synthesis and molecular structure – arene η^2-C_2 and tetrel bonding

Vânia Denise Schwade [a,*], Luana Floriano [a], Antonio Frontera [b], Asmet N. Azizova [c,d], Ghodrat Mahmoudi [e,f]

[a] Department of Chemistry, Natural and Exact Sciences Centre, Federal University of Santa Maria, Av. Roraima, 1000, Santa Maria, RS 97105-900, Brazil
[b] Departament de Química, Universitat de les Illes Balears, Crta. de Valldemossa km 7.5, 07122 Palma de Mallorca, Baleares, Spain
[c] Azerbaijan Medical University, Scientific Research Centre (SRC), A. Kasumzade, St. 14. AZ 1022, Baku, Azerbaijan
[d] Scientific Research Center, Baku Engineering University, Khirdalan, Hasan Aliyev str. 120, Absheron, AZ0101, Azerbaijan
[e] Department of Chemistry, Faculty of Science, University of Maragheh, P.O. Box 55181-83111, Maragheh, Iran
[f] Department of Chemistry, Dogus University, Dudullu-Ümraniye, Istanbul, 34775, Türkiye

ARTICLE INFO

Keywords:
Pb(II) complexes
Tetrel bonds
Benzoylhydrazone
Crystal engineering

ABSTRACT

Four Pb(II) complexes with a hydrazone ligand obtained from 2-acetylpyridine and benzhydrazide were prepared by using Pb(II) acetate, nitrate and carbonate salts: $[Pb(HL)_2(NO_3)_2]$ (**1**), $[Pb(L)(CH_3CO_2)]_n$ (**2**), $[Pb(L)_2]_n$ (**3**), and $[Pb(L)(NO_2)]_n$ (**4**). Compound **4** was obtained from reaction of Pb(II) nitrate and addition of nitrite. Pb(II) carbonate reacts only by heating in *N,N*-dimethylformamide, producing compound **3**. Structural analysis by single-crystal X-ray diffraction reveals that compound **1** exhibits a holodirected geometry with the ligand coordinated in its neutral form, whereas compounds **2**–**4** display hemidirected geometries with stereochemically active lone pairs and anionic hydrazonate ligands. The supramolecular architectures of these complexes are stabilized by non-covalent interactions, including hydrogen bonds and tetrel bonds. DFT calculations (MEP, QTAIM, and NCIplot) were employed to analyze the self-assembled dimers of the homoleptic complex **3** and its polymorph **3A**. The theoretical results corroborate the existence of Pb•••N(azomethine) tetrel bonds in compound **3** and uncover a novel Pb•••η^2-C_2(arene) interaction in polymorph **3A** and **4**. For compound **4**, the analysis additionally identifies the formation of strongly bound antiparallel π-stacked dimers driven by electrostatic complementarity. Energetic analysis indicates significant dimerization energies for these assemblies, highlighting the crucial role of these specific non-covalent interactions in the crystal packing. The compounds were further characterized by elemental analysis, FT-IR, NMR and diffuse reflectance spectroscopies.

1. Introduction

N-Acylhydrazones are a distinctive subclass of Schiff bases, structurally defined by the –CO–NH–N=CH– moiety. The weak acid-base properties of their derivatives are governed by the interplay between the azomethine nitrogen (–N=CH–) and the adjacent amide group (–CO–NH–) [1]. They form complexes with Group 14 elements [Si, Ge, Sn, Pb] in (+II) and (+IV) oxidation states, with exception of Si (oxidation state +IV). The NO donor set has strong chelating properties being known complexes of Si through Pb [2–5]. Two chelates can be formed with addition of an appropriate oxygen or nitrogen donor [6,7].

The structural chemistry of lead(II) complexes is largely governed by the electronic configuration of the metal ion, specifically the presence of the valence $6s^2$ electrons [8]. These electrons, often referred to as the inert lone pair, can exhibit varying degrees of stereochemical activity. When the lone pair is stereochemically active, it occupies a specific position in the coordination sphere, repelling the ligand donor atoms. This results in a distribution of bonds that covers only a portion of the coordination sphere, leaving a discernible gap or void. This geometry is classically defined as *hemidirected* [9]. Typical examples of homoleptic Pb(II)-hydrazone complexes contain the metal center with coordination number six [10,11]. In these complexes, each ligand creates two chelating rings through the *N,N',O*-donors, resulting in *e.g.* distorted trigonal prismatic geometry [11]. In contrast, when the lone pair is inactive or when the high coordination number forces a symmetric distribution of ligands, the geometry is termed *holodirected*, and the

* Corresponding author.
E-mail address: vaniaschwade@ufgd.edu.br (V.D. Schwade).

https://doi.org/10.1016/j.molstruc.2026.146840
Received 8 April 2026; Received in revised form 24 May 2026; Accepted 13 June 2026
Available online 15 June 2026

ligands are arranged evenly around the metal center [9]. Thinking on Pb (II)-hydrazone complexes, the number of examples is very reduced; otherwise such arrangement is achieved only taking in account the tetrel bonds, *e.g.* heteroleptic compounds containing nitrate and halide ligands [12,13].

The structural void present in hemidirected complexes is of significant interest in crystal engineering, as it frequently acts as an electrophilic site capable of engaging in secondary non-covalent interactions, such as tetrel bonds [9]. Lead tetrel bonds may be qualitatively described as existing when there is evidence of a net attractive interaction between an electrophilic region associated with lead in a molecular entity and a nucleophilic region in another, or the same, molecular entity [14]. Comprehension of the Pb(II) coordination at a molecular level is, thus, ideally recommended by the help of theoretical computations. The bonding pattern is very important as the tendency of the lead(II) cation to exhibit a gap in its coordination sphere seems strongly linked to the cation's toxicity (i.e., the well-known lead poisoning) [15]. The coordination properties of lead is crucial for the design of selective chelation therapy agents, and the development of efficient chelating agents for the remediation of polluted water and soil [16].

We have observed before that 2-acetylpyridine benzoylhydrazone (HL, Fig. 1) reacts with lead(II) thiocyanate and the $[Pb(HL)(NCS)_2]$ complex is formed. Pb•••S tetrel bonds and H-bonds were observed in the analysis of the molecular structure in the solid-state [7]. In the same work, we observed that deprotonation occurs within recrystallization in DMF solution, yielding [Pb(L)(SCN)]. Pb•••N tetrel bonds were then formed. In the present work, we are interested in the study of the resulting coordination compounds of HL with lead(II) nitrate and acetate salts.

In addition to the structural characterization, we present a detailed theoretical study using DFT calculations to analyze the non-covalent interactions governing the crystal packing of the homoleptic complex **3** and its polymorph **3A**. We focus on corroborating the existence of tetrel bonding interactions, specifically the unconventional Pb•••N (azomethine) contact in compound **3**, which exhibits a distance slightly beyond the van der Waals limit, and the Pb•••η^2-C_2(phenyl/pyridyl) interaction in compounds **3A** and **4**. To our knowledge, this latter interaction involving the phenyl or pyridyl ring as a donor to the lead(II) center has not been previously analyzed in this class of compounds.

2. Results and discussion

Four coordination compounds with Pb^{2+} salts were obtained with 2-benzoylpyridine benzoylhydrazone (HL) as ligand. The simple mixture of the Pb^{2+} nitrate and acetate salts with HL in methanol (Scheme 1) produced compound $[Pb(HL)_2(NO_3)_2]$ (**1**) and $[Pb(L)(CH_3CO_2)]_n$ (**2**). The use of NEt_3 as supporting base in the reaction of Pb^{2+} acetate produced compound $[Pb(L)_2]_n$ (**3**). We have also observed that the addition of sodium nitrite to the mixture of Pb^{2+} nitrate and HL produces $[Pb(L)(NO_2)]_n$ (**4**). The objective of the addition of nitrite was the preparation of an analog of compound of **2**, replacing acetate by nitrite and compare their molecular and supramolecular structures. Both co-ligands were expected to coordinate through their *O,O*'-donors. Compound **1** is white while compounds **2** − **4** are yellow.

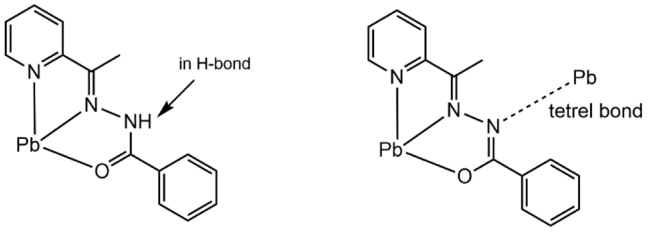

Fig. 1. Chemical structure of 2-acetylpyridine benzoylhydrazone (HL) and its known coordination mode toward Pb(II) [7].

Compounds **1**–**4** are soluble in methanol. If the synthesis are performed with a higher amount of solvent, precipitation will be not observed within the reaction time (2 h). However, this approach can be used to obtain good single-crystals for structural analysis, particularly compounds **2** and **3** that have a needle shape. Compound **1** starts to precipitate within 2 h of reaction, being collected by filtration after 2.5 h. From the mother liquor, good quality blocks of **1** were formed. Crystals of sufficient quality of compound **4** were formed from the mother liquor as well. For all compounds, the solids that were collected at the end of the reaction time were used for quantification and spectroscopic characterization.

We have also performed a reaction of Pb^{2+} carbonate with HL in DMF under heating at 90–95 °C. Compound **3** crystallized from the solution as yellow rectangular needles, in between of few crystals of polymorph **3A** (yellow blocks) (Scheme 2). In the same solvent, at room temperature, the replacement of the carbonate salt by Pb^{2+} acetate produced compound **2** as yellow precipitate (and not **3**, which could be also expected), even though a 1:2 (Pb^{2+}:HL) stoichiometry was used.

2.1. *Molecular structures*

In compound **1**, the hydrazone ligands coordinate in a neutral form through the *N,N*',*O* donor atoms. Two five-membered chelate rings were formed. The C−O bond lengths of 1.233(3) Å (Table S3) are close to free ligand (1.219(2) Å [17]) thus proving the neutral coordination. For charge compensation, there are two nitrate ions. Both hydrazone and nitrate ligands are in *trans* position (Fig. 2). The Pb center is ten-coordinated, but one nitrate ligand has longer Pb−O distances [2.877(3)−2.9161(6) Å, Table 1], which can be better described as interactions. For comparison, the other nitrate ligand is coordinated with Pb−O bond lengths of 2.641(2) and 2.731(2) Å. The coordination sphere has primarily the N_4O_4 set, which expands to N_4O_6 set. Therefore, a holodirected geometry is observed considering both the covalent and non-covalent bonds. The Pb−N bond lengths of the hydrazone ligand range from 2.725(2) to 2.875(2) Å, which are longer than in the previous compound $[Pb(HL)(NCS)_2]$ (2.662(3) and 2.641(3) Å) [7]. The Pb−N bond lengths in $[Pb(HL1)_2(NO_3)_2]$ (HL1 = 2-benzoylpyridine 4-phenylsemicarbazide) (2.6832(16)−2.7978(17) Å) [12] are closer to those observed in **1**.

A one-dimensional arrangement results from N−H•••O hydrogen bonds, in the solid-state (Fig. S4). Such H-bonds have been observed before in $[Pb(HL1)_2(NO_3)_2]$ [12]. Different situation occurs in [Pb(HL2)$(NO_3)_2$] (HL2 = 2-acetylpyridine isonicotinoylhydrazone) where the single hydrazone ligand in the complex enables the hemidirected structure. A 1D extended chain is then constructed by secondary Pb•••$O_{nitrate}$ interactions [13].

Compounds **2** and **3**/**3A** contain a hydrazonate ligand. The deprotonation was promoted by the acetate or by the use of supporting base NEt_3, or even by the carbonate in heating reaction condition. Compounds **2** and **4** are heteroleptic complexes (with an additional acetate or nitrite ligand) (Fig. 3b) while **3**/**3A** is homoleptic (Fig. 4). Compounds **2** and **4** are less symmetric and have their structures adequately calculated in monoclinic space groups. Compounds **3**/**3A** have higher symmetry, with their structures calculated in orthorhombic space groups. Across the Pb center and, indeed, the lone pair, there is a 2-fold rotation axis (in **3**) and a 2-fold rotation axis plus a glide plane parallel to the axis (in **3A**).

In compounds **2** and **4**, the hydrazonate ligand coordinates through the pyridinic nitrogen atom N(1), azomethine nitrogen atom, N(2), and amidate oxygen atom, O(1), while in **3**/**3A** they coordinate exclusively through N(2) and O(1). The bonding parameters are in good agreement with the coordinating pattern of a C═N−N═C–O moiety: C(8)–O(1) in 1.28–1.29 Å range, and C(8)–N(3) in 1.33–1.34 Å range (Table S3). The acetate ligand in compound **2** coordinates in asymmetrical way with

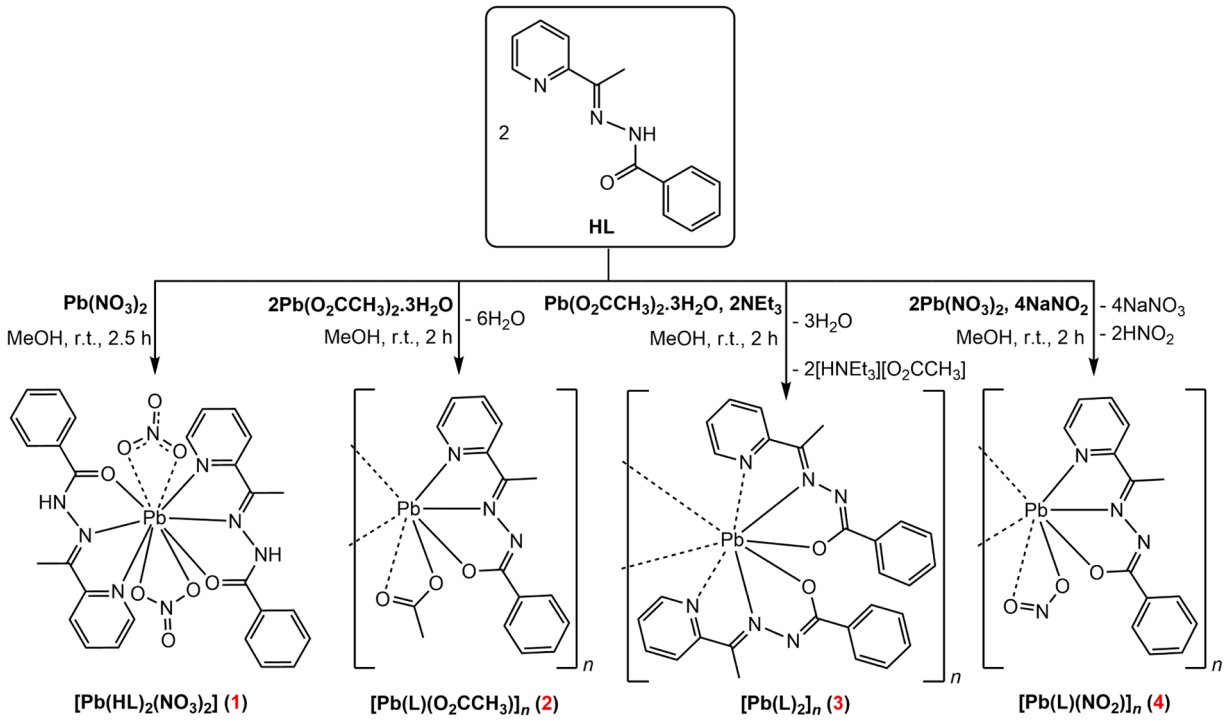

Scheme 1. Synthesis of the Pb(II) complexes, in methanol.

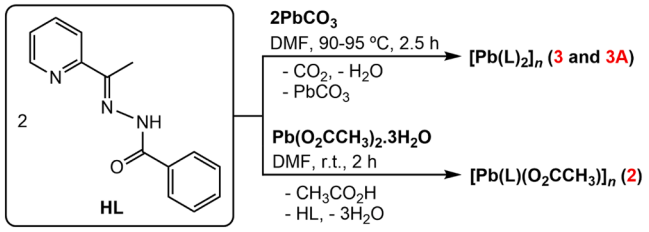

Scheme 2. Reactions of HL and Pb^{2+} carbonate and acetate, in DMF.

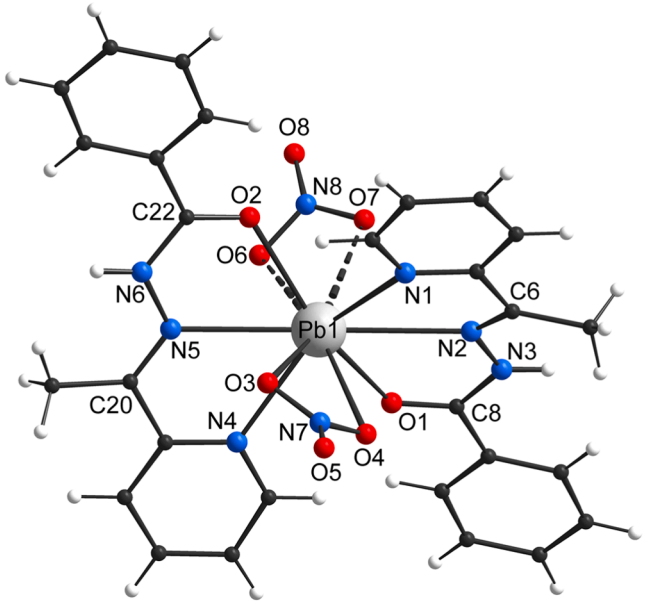

Fig. 2. Molecular structure of compound **1**.

Table 1
Selected bond lengths (in Å) for compounds **1, 2, 3/3A** and **4**.

	1	2	3	3A	4
Pb(1)-N (1)	2.794(2)	2.559(2)	2.843 (2)	2.822(2)	2.532(3)
Pb(1)-N (2)	2.875(2)	2.439(3)	2.571 (2)	2.5763 (19)	2.396(3)
Pb(1)-N (4)	2.725(2)	–	–	–	–
Pb(1)-N (5)	2.804(2)	–	–	–	–
Pb(1)-O (1)	2.637(2)	2.351(2)	2.364 (2)	2.3165 (18)	2.361(2)
Pb(1)-O (2)	2.660(2)	2.331(2) acetate	–	–	2.370(3) nitrite
Pb(1)-O (3)	2.641(2) nitrate	2.748(3) acetate	–	–	2.807(3) nitrite
Pb(1)-O (4)	2.731(2) nitrate	–	–	–	–
Pb(1)-O (6)	2.877(3) nitrate	–	–	–	–
Pb(1)-O (7)*	2.9161(6)/2.8867 (7) nitrate	–	–	–	–

* The second value corresponds to the Pb(1)-O(7B) bond. Atoms O(7) and O(7B) are from a disorder.

Pb–O bond lengths of 2.331(2) and 2.748(3) Å (Table 1) being better described as monodentate coordination with an additional interaction (Fig. 3a). The C–O bond lengths in acetate are also asymmetrical [C(15)–O(2) = 2.282(4); C(15)–O(3) = 2.242(4) Å], corroborating with the coordination mode. Anyway, the acetate coordination can be further comprehended as pseudo bridging bidentate mode (Fig. 3b). Similarly, in compound **4** the coordination of the nitrite ligand is asymmetrical (Pb–O bond lengths of 2.370(3) and 2.807(3) Å, Table 1). The N–O bond lengths in the nitrite ligand are N(4)–O(2) = 1.279(4) and N(4)–O(3) = 1.236(4) Å.

The 'coordination' by the pyridyl nitrogen atom N(1) is somewhat atypical for compounds **3/3A**. The Pb–N(1) bond lengths in **3/3A** (2.843(2)/2.822(2) Å, Table 1) are considerably longer than in **2** (2.559

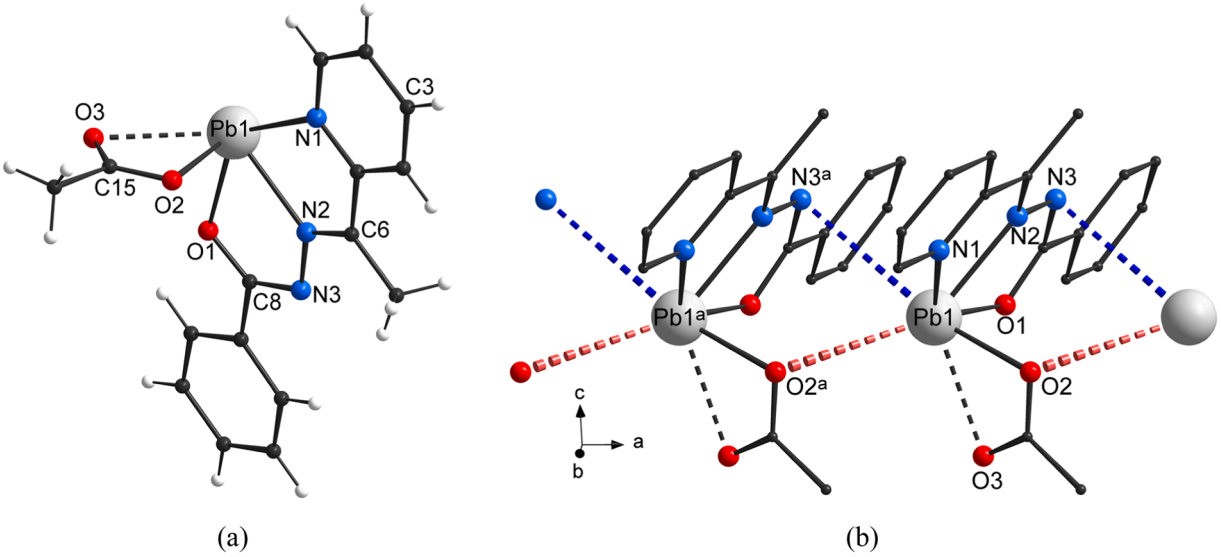

Fig. 3. (a) Molecular structure of compound **2**; (b) Solid-state arrangement of compound **2**. Hydrogen atoms were omitted for clarity. Symmetry operator: [a] $x - 1$, y, z.

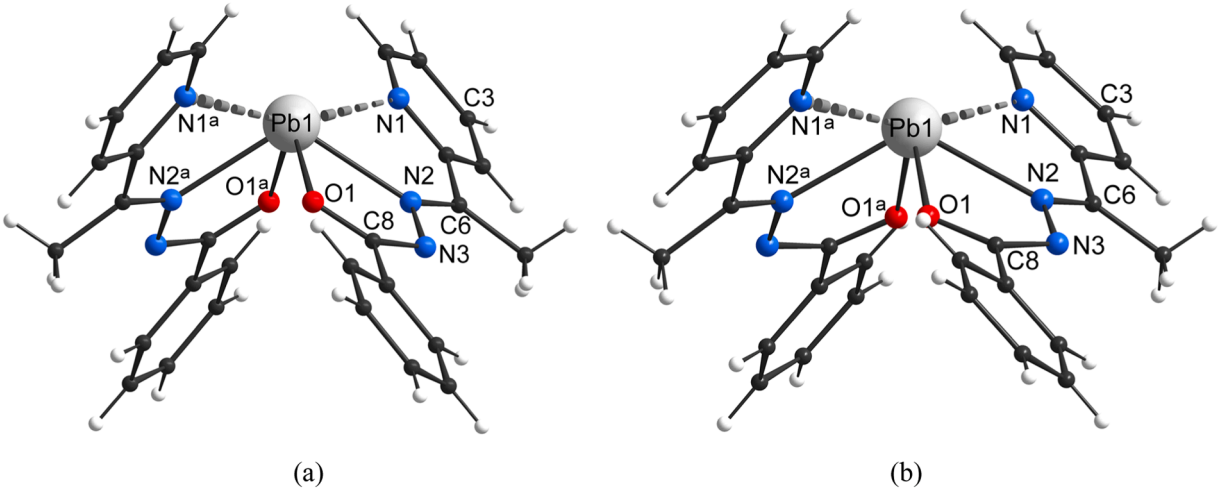

Fig. 4. Molecular structures of compound (a) **3**; (b) 3A. Symmetry operator: [a] $[-x + 1.5, -y + 0.5, z]$ for 3; $[-x + 1, y, -z + 0.5]$ for 3A.

(2) Å) and **4** (2.532(3) Å). In **3**/**3A** these bonds are better considered as Pb•••N interactions due to the Pb−N(1)−Cg (Cg = centroid of the pyridyl ring) angles. Since pyridyl is a planar substituent, we can analyze it by the Pb(1)−N(1)−C(3) angles. The values calculated by PLATON program are 156.53(1)° and 160.78(1) for **3** and **3A**, respectively, which are quite far from 180°, which reflects the 'weak' donation of the electron pair from N(1) to Pb(1). For comparison, in **2** and **4**, the related angles are 177.72(1)° and 174.60(1)°, respectively. Fig. S5 illustrates the clear differences in the angle resulted from N(1) coordination/interaction with Pb. In principle, no apparent reason would be expected for this observation since all compounds show the inert pair effect in the coordination geometry. A more detailed comment will be found in the DFT studies section.

In all complexes, hemidirected coordination geometries are observed, based on the clear gap produced on the asymmetrical distribution of the coordinated atoms from the ligands. In compound **2**, the coordination sphere has primarily the N_2O_2 set, which expands to N_3O_4 set. In compounds **3**/**3A** and **4**, the N_2O_2 set expands to N_6O_2 (**3**), $N_4O_2(\eta^2-C_2)_2$ (**3A**) and $N_3O_3(\eta^2-C_2)$ (**4**).

The gap in the coordination spheres of the molecular structures of compounds **2** (Fig. 3a), **3** (Fig. 4a) and **4** (Fig. 7a) is partially fulfilled by tetrel bonds (Pb•••O and/or Pb•••N interactions). Fig. 3b and Fig. 5 present the one-dimensional arrangement in **2** and **3**, as the crystal

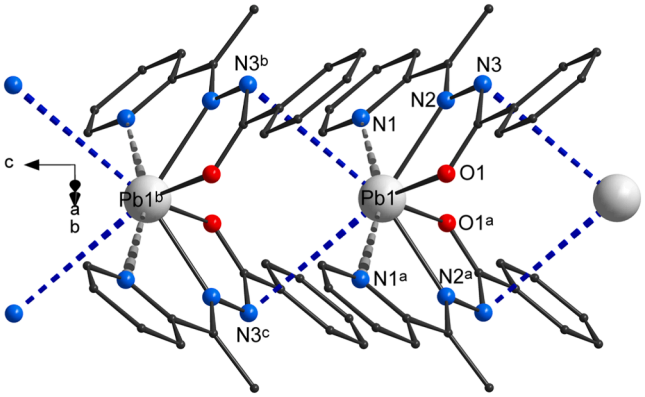

Fig. 5. View of the pseudo-polymer **3**. Hydrogen atoms were omitted for clarity. Symmetry operators: [a] $-x + 1.5, -y + 0.5, z$; b $x, y, z + 1$; c $-x + 1.5, -y + 0.5, z + 1$.

formats (thin rectangular blocks/needles) strongly suggest; thus, these compounds are pseudo-polymers. Many other authors find out the formation of 1D extended chains or a 2D extended layers for hydrazone-containing Pb(II) compounds via such interactions [18,19]. The Pb•••N distances are 3.382(2) and 3.929(2) Å (Table 2). In **3**, although the distance is on the limit of the van der Waals radii sum of Pb and N (3.9 Å [20]), the DFT analysis corroborates the tetrel bonds formation, as detailed below. In **2**, the Pb•••O distance is equal to 3.460(3) Å, which is in between the sum of the van der Waals radii of the corresponding elements (3.85 Å) [20]. According to our knowledge, compound **2** is the first example of a heteroleptic complex containing acetate having both Pb•••N and Pb•••O tetrel bonds. This may be achieved due to the absence of donor atom(s) in the aromatic group of the –C(O)R fragment of the hydrazonate ligand. When the ligand contains a donor atom in this fragment, normally a nitrogen atom, Pb•••N [21] or Pb•••N and π−π interactions [22] are favored.

Homoleptic Pb(II) complexes with hydrazones derived from 2-acetylpyridine or 2-pyridylaldehyde and arylhydrazides are scarce. Based on a search on CSD (Cambridge Structure Database) we could find only one example, prepared by Chung et al. *via* sonochemical synthesis (and branched tube method for crystals). The ligand of the complex is 2-pyridinecarbaldehyde isonicotinoylhydrazonate [10]. The authors describe the complex as discrete, with coordination number of six for the Pb(II) atom and asymmetrical hemidirected geometry. They comment about π–stacking interactions (distance of 3.433 Å) allowing the discrete structure to form a 1D network. No comments were made about tetrel Pb•••N bonds. However, our analysis on the CIF file of this compound indicates that tetrel bonds may be present. They probably refer to the 'weak supramolecular interactions' described by the authors forming the 3D architecture. Compared to **3**/**3A**, the Pb−N bond lengths with the pyridyl and azomethine nitrogen atoms are close (2.872(3) and 2.552(3) Å [10], respectively). Interesting is that the Pb−N(pyridyl)−C(pyridyl) angle is 168.4°, which is closer to 180° when compared with **3**/**3A**.

The analysis of the solid-state structure of compound **3A** reveals unexpected Pb•••η^2−C_2 interactions. Carbon atoms C(12) and C(13) from the phenyl rings of neighbouring metal complexes fulfill the hemidirected coordination sphere of the Pb(II) ion in the complex (Fig. 6). It results in a two-dimensional network (Fig. S6). Since the crystals were easily obtained and are very stable, DFT studies were performed to corroborate the formation of such interaction. The Pb−C (12) and Pb−C(13) distances are 3.495(2) and 3.540(2) Å. Table 2 lists all the distances of the intermolecular interactions of all compounds.

Compound **4**, at first inspection, is a pseudo-dimer by non-covalent interactions (two Pb•••N tetrel bonds and two π−stacking interactions; Fig. 7b). The Pb•••N distances are 3.227(3) Å (Table 2). The π−π interactions are within the pyridyl and phenyl rings. The Cg-Cg distances are 3.5734(17) Å, with slippage of 1.069 Å. These two types of interactions producing a pseudo-dimer was observed before for [Pb(L)(SCN)] [7]. Similar case was observed before in a complex with

Table 2
Solid-state intermolecular interactions (Å) in compounds **1**, **2**, **3**/**3A**, and **4**.

	1	2	3	3A	4
Pb•••N (azomethine)	–	3.382 (2)	3.929 (2)	–	3.227(3)
Pb•••O(acetate)	–	3.460 (3)	–	–	–
Pb•••η^2-C_2(phenyl)	–	–	–	3.495(2), 3.540(2)	–
Pb•••η^2-C_2(pyridyl)	–	–	–	–	3.476(2), 3.652(3)
N-H•••O(nitrate)	2.955(3), 3.305(3)	–	–	–	–
Coordination number*	10	7	8	8	7

*including the Pb•••X (X = N, O, C) interactions. The η^2−C_2 bonds were counted as a single interaction.

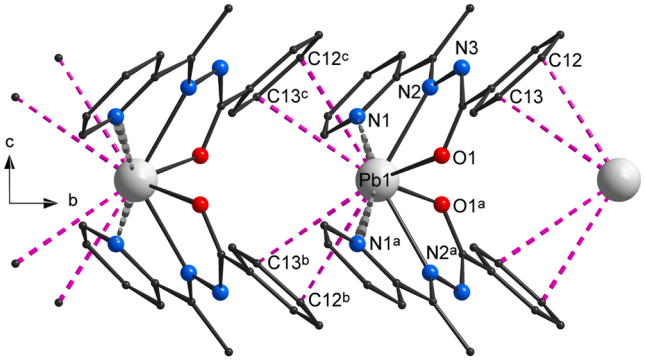

Fig. 6. View of the pseudo-polymer **3**A along the [100] direction. Hydrogen atoms were omitted for clarity. Symmetry operators: [a] $-x+1, y, -z+0.5$; b $x-0.5, y-0.5, -z+0.5$; c $-x+1.5, y-0.5, z$.

2-acetylpyridine isonicotinohydrazide as ligand in which the aza N-atom approaches the Pb(II) and forms a Pb•••N tetrel bond (in addition, the 4-pyridyl N-atom approaches a second tetrel bond) [23]. In **4**, the O(3)−Pb(1)−N(3)[a] angle of 167.48(1)° (from PLATON) suggests the tetrel bonding interaction. As comparison, the O(2)−Pb(1)−N(3)[a] angle in compound **2** is 160.28(1)°. However, a void is still present in **4**, allowing further interactions. Pb•••η^2−C_2 interactions involving C(2) and C(3) carbon atoms from the pyridyl rings of neighbouring metal complexes (Fig. S7) are observed. DFT section will contain the studies on the formation of such interaction. It is worth to highlight that Pb•••η^2−C_2 interactions in compound **4** happens with pyridyl ring carbon atoms, while in **3A** they occur with phenyl ring carbon atoms.

2.2. *DFT analysis* ***on tetrel bonds in compounds 3/3A and 4***

The experimental X-ray diffraction analysis of compounds **3**/**3A** and **4** reveals supramolecular architectures likely stabilized by specific non-covalent interactions involving the lead(II) center. To characterize these contacts and quantify their contribution to the crystal packing, we performed DFT calculations on the self-assembled dimers derived from the X-ray coordinates. First, the molecular electrostatic potential (MEP) surfaces were computed to identify the location and intensity of the σ-holes (a region of lower electronic density on the extension of a covalent bond) on the hemidirected Pb atom, verifying its capability to participate in tetrel bonding. This was followed by a combined QTAIM (Quantum Theory of Atoms in Molecules) and NCIplot (Non-Covalent Interaction plot) analysis to unequivocally characterize the bond critical points and attractive regions associated with the Pb•••N and Pb•••η^2-C_2 interactions. Finally, an energetic analysis was conducted to estimate the dimerization energies and assess the stability provided by these supramolecular contacts.

The molecular electrostatic potential (MEP) surface of the monomeric [Pb(L)$_2$] unit was computed to evaluate the charge distribution and identify the potential donor and acceptor sites driving the supramolecular assembly (Fig. 8a). The MEP map reveals a significant anisotropy around the lead(II) center, consistent with a hemidirected geometry influenced by a stereochemically active $6s^2$ lone pair. The Pb atom exhibits two symmetric σ-holes located on the equatorial belt perpendicular to the coordination plane. These electrophilic regions are characterized by a positive potential of +12.6 kcal/mol, indicating their capability to participate in attractive interactions with electron-rich moieties. Regarding the nucleophilic sites, the MEP global minimum is located at the oxygen atoms of the hydrazonate groups (–38.6 kcal/mol), while the aromatic protons of the pyridyl rings represent the global maximum (+22.3 kcal/mol). Crucially for the supramolecular analysis, the azomethine nitrogen atoms exhibit large negative potentials (–35.8 and –28.2 kcal/mol), confirming their strong Lewis base character. Furthermore, the MEP values over the phenyl rings are also negative,

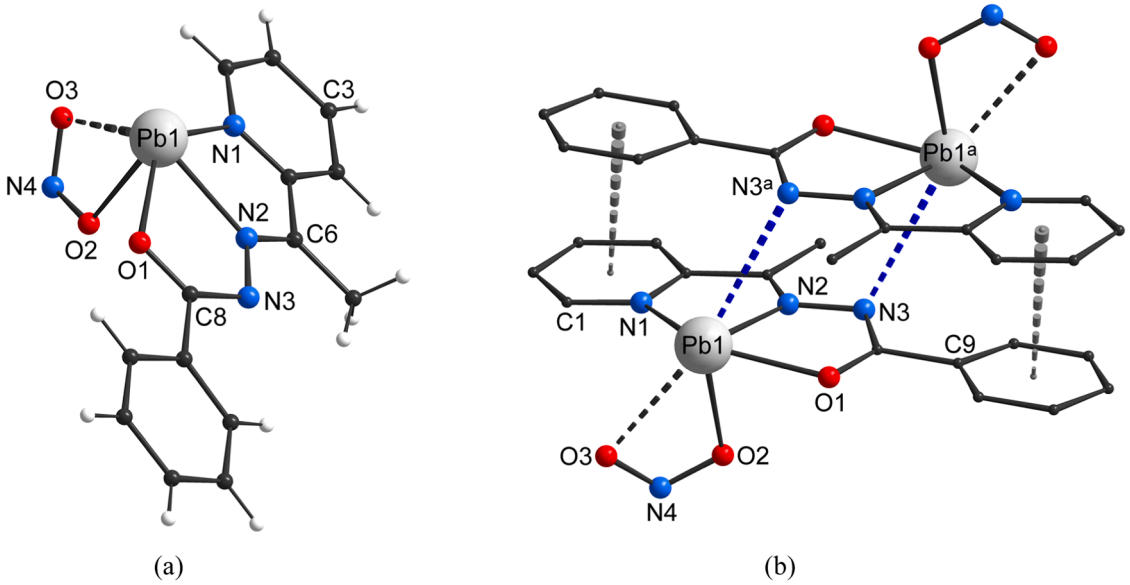

Fig. 7. (a) Molecular structure of compound **4**; (b) Pseudo-dimeric structure of compound **4**. Hydrogen atoms were omitted for clarity. Symmetry operator: [a] $-x+1, -y, -z+1$; [b] $-x+1.5, y-0.5, -z+0.5$.

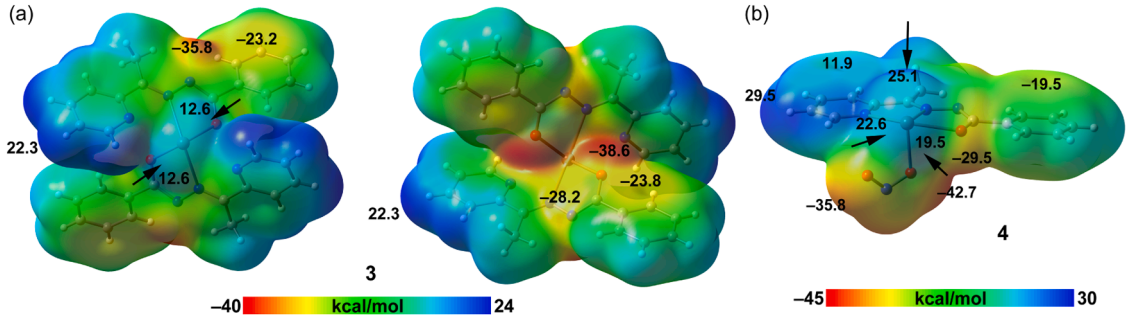

Fig. 8. Molecular electrostatic potential (MEP) surface of compound **3** (isosurface 0.001 a.u.) in two opposite orientations (a) and **4** (b). The energies at selected points are indicated in kcal/mol. Red and blue regions correspond to negative and positive potentials, respectively. The arrows indicate the location of the σ-holes.

ranging from –23.2 to –23.8 kcal/mol, which suggests the aromatic system can act as a donor in C–H•••π or tetrel bonding interactions. In the case of the heteroleptic complex **4** (Fig. 8b), the MEP global maximum is located at the aromatic H-atoms of the coordinated pyridyl rings (+29.5 kcal/mol) and the minimum at the nitrite ligand (−42.5 kcal/mol). Similar to the homoleptic complexes, the MEP is also positive at the Pb atom, showing anisotropy and three preferential directions (σ-holes) with energies ranging from +19.5 to +25.1 kcal/mol. An interesting issue is observed in the planar extended surface opposite to the nitrite ligand: (i) the MEP is negative over the phenyl ring and its fused chelate ring, and (ii) positive over the pyridyl ring at its fused chelate ring.

This charge distribution provides a robust rationale for the experimental structures. The presence of two symmetric σ-holes on the Pb atom and the availability of electron-rich N(azomethine) and phenyl groups align perfectly with the formation of the self-assembled dimers. Specifically, the σ-hole•••N interaction explains the assembly in compound **3** (Fig. 5), while the interaction between the σ-hole and the negative potential of the phenyl ring corroborates the formation of the Pb•••η^2-C_2 bonds observed in polymorph **3A** (Fig. 6). For compound **4**, the three σ-holes identified on the lead(II) center are consistent with its ability to engage in multiple non-covalent contacts within the crystal lattice. Furthermore, the electrostatic complementarity between the positive and negative regions of the planar extended surfaces effectively drives the formation of the antiparallel π-stacked dimers (Fig. 7b), where the positive pyridyl fragment of one monomer overlaps with the negative phenyl fragment of the neighbouring unit.

To further characterize the nature of the interactions within the crystal lattice, a combined QTAIM and NCIplot analysis was performed on the self-assembled dimer of compound **3** (Fig. 9). It should be noted that the proximity of the two monomers generates a complex and dense network of bond critical points (BCPs) and bond paths. Therefore, for the sake of clarity, the QTAIM distribution shown in Fig. 9a is a partial representation, displaying only the BCPs associated with the tetrel bonds and hydrogen bonds, while omitting others to avoid overcrowding the figure. To provide the whole picture of the non-covalent interactions, including dispersive forces, we relied on the NCIplot analysis (Fig. 9b).

Focusing on the QTAIM results, the intramolecular Pb•••N(pyridyl) contacts (green BCPs) exhibit a low electron density ($\rho = 0.0249$ a.u.) and a potential-to-kinetic energy density ratio (–G/V) of 0.98. These values, along with the discrete light blue isosurfaces in the NCIplot, unequivocally confirm the non-covalent nature of these intramolecular tetrel bonds. Regarding the intermolecular assembly, the analysis confirms the existence of the Pb•••N(azomethine) tetrel bonds predicted by the MEP study. These are characterized by specific bond paths and BCPs (red spheres) connecting the Pb atoms to the azomethine nitrogen atoms. The NCIplot characterizes these long contacts (3.99 Å) as weak, evidenced by the green Reduced Density Gradient (RDG) isosurfaces.

Furthermore, the dimer is reinforced by C—H•••O hydrogen bonds involving the pyridyl C—H groups and the hydrazonate oxygen atoms.

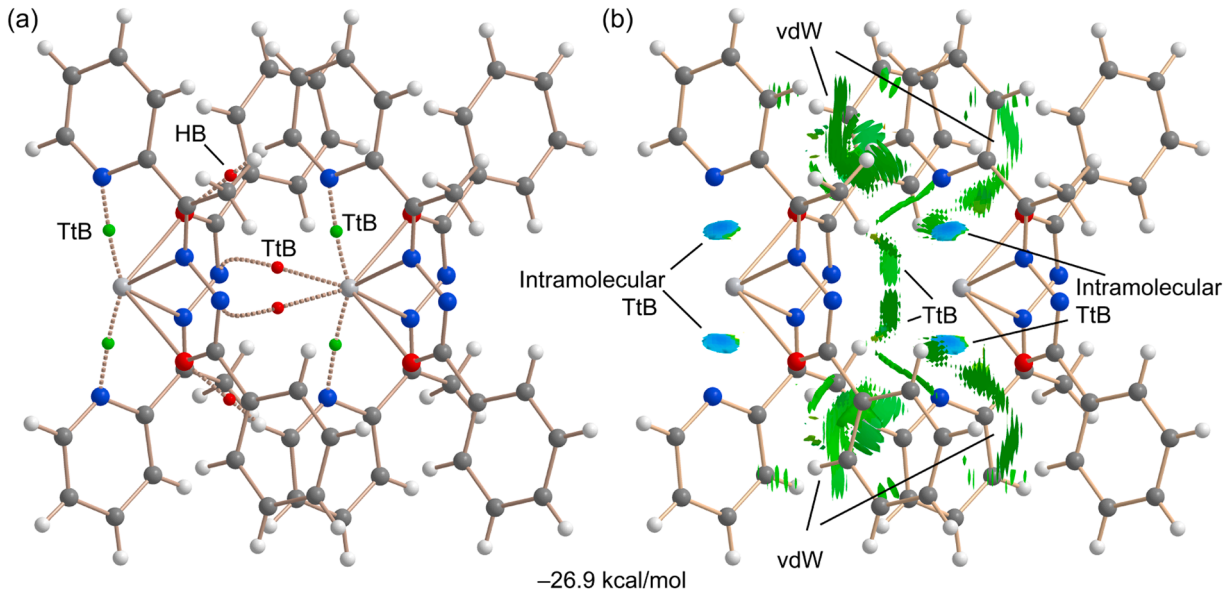

Fig. 9. (a) QTAIM analysis of the self-assembled dimer of **3**. This is a partial representation showing only selected bond critical points (spheres) and bond paths (dashed lines) for clarity; intermolecular BCPs are shown in red, and intramolecular Pb•••N BCPs are shown in green. (b) NCIplot analysis of the same dimer providing the complete interaction picture; light blue disks correspond to stronger non-covalent interactions (intramolecular tetrel bonds), while green surfaces indicate weaker interactions (intermolecular tetrel bonds, H-bonds, and van der Waals forces).

While the simplified QTAIM diagram highlights these specific interactions, the NCIplot reveals the full extent of the supramolecular assembly: large green isosurfaces are observed between the aromatic rings, evidencing the existence of extensive van der Waals interactions (π•••π and C—H•••π) that were omitted in the QTAIM graph. The combination of these tetrel bonds, hydrogen bonds, and van der Waals contacts results in a large dimerization energy of –26.9 kcal/mol, confirming the significance of this assembly in the solid state.

A similar analysis was performed for the self-assembled dimer of polymorph **3A** to investigate the Pb•••η^2-C_2 interaction (Fig. 10). The QTAIM distribution (Fig. 10a) reveals a bond path connecting the Pb atom to one carbon atom of the phenyl ring, characterizing the Pb•••C contact. Notably, the bond path extends from the Pb atom toward the center of the C—C bond and subsequently bends toward the carbon atom that is geometrically closer to the lead center. The specific Pb•••η^2-C_2 nature of this interaction is more clearly defined by the NCIplot analysis (Fig. 10b), where the green RDG isosurface spatially embraces the region between the Pb atom and the C—C bond of the aromatic ring.

Regarding the intramolecular tetrel bonds between the pyridyl nitrogen and Pb atoms (represented by green BCPs in Fig. 10a), the calculated QTAIM parameters are very similar to those observed in compound **3**. The electron density is 0.0261 a.u. and the potential-to-kinetic energy density ratio (-G/V) is 0.97. These values, combined with the presence of distinct blue RDG disk isosurfaces in the NCIplot, confirm the non-covalent nature of these intramolecular contacts. The NCIplot also highlights green isosurfaces between the aromatic rings, indicating the contribution of van der Waals forces to the assembly.

Finally, the dimerization energy for this assembly is –15.2 kcal/mol. This value is significantly smaller than that calculated for the dimer of **3** (–26.9 kcal/mol). This reduction in stability is attributed to the presence of only one Pb•••η^2-C_2 interaction in this specific dimer, the absence of the short intermolecular C—H•••O hydrogen bonds observed in **3**, and a reduced extent of van der Waals interactions as evidenced by the smaller area of green RDG isosurfaces between the molecules.

The QTAIM analysis of mononuclear compound **4** reveals an interesting binding mode for the nitrite ligand. While one oxygen atom forms a standard coordination bond with the Pb center, the other oxygen atom is engaged in an intramolecular tetrel bond, characterized by a green

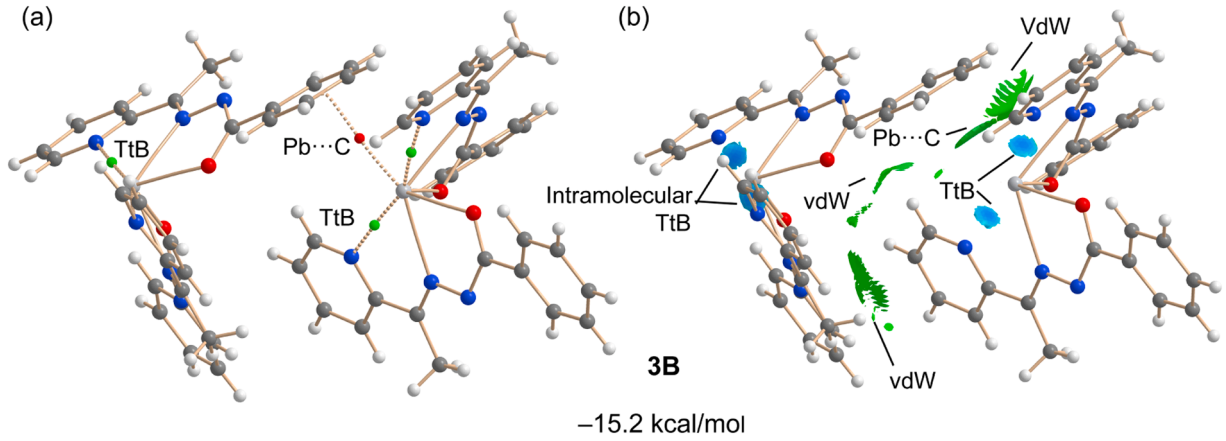

Fig. 10. (a) QTAIM analysis of the self-assembled dimer of **3A** showing the bond critical points (spheres) and bond paths (dashed lines) associated with the Pb•••C and intramolecular interactions. (b) NCIplot analysis of the same dimer highlighting the Pb•••η^2-C_2 interaction; light blue disks correspond to stronger non-covalent interactions (intramolecular tetrel bonds), while green surfaces indicate weaker interactions (intermolecular Pb•••C and van der Waals forces).

BCP. This is analogous to the intramolecular Pb•••N interaction observed in compound **3**. The QTAIM parameters at this BCP (ρ = 0.0247 a.u. and -G/V = 1.01) confirm the non-covalent, weak nature of this interaction.

Fig. 11 illustrates the QTAIM and NCIplot analyses for two different intermolecular dimers of compound **4**. For the self-assembled π-stacked dimer, the QTAIM analysis (Fig. 11a) reveals a large number of BCPs interconnecting the monomers. These BCPs characterize extensive π-stacking interactions involving the phenyl and pyridyl rings, as well as interactions between the chelate rings (CR•••CR). Notably, the Pb atom is connected via bond paths to one N-atom of a five-membered chelate ring and one C-atom of the electron-rich phenyl ring of the adjacent molecule, indicating the participation of Pb•••C contacts in the binding mechanism. The NCIplot analysis (Fig. 11b) exhibits an extended and continuous green RDG isosurface between the π-systems of both molecules, further confirming the strong complementarity and the multicentric nature of the interaction. The calculated dimerization energy is large (–22.5 kcal/mol), consistent with the antiparallel orientation dictated by electrostatic complementarity, where the positive region of one molecule interacts with the negative region of the other.

Fig. 11c displays a second dimer exhibiting a Pb•••η^2-C_2 interaction. The QTAIM analysis shows that the Pb atom is connected by a single bond path and BCP to the C-atom of the phenyl ring with the shortest Pb-C distance. This interaction is assisted by an additional C—H•••O contact between an aromatic C—H bond of the coordinated pyridyl group and the O-atom of the hydrazide group. This aligns with the MEP analysis, which identified the pyridyl protons as good H-bond donors. The η^2-hapticity of the Pb•••C interaction is clearly evidenced by the NCIplot analysis (Fig. 11d), where a green isosurface embraces the space between the Pb atom and one of the aromatic C—C bonds. The calculated dimerization energy is moderately strong (−9.4 kcal/mol), supporting the significance of this supramolecular assembly in the solid state of compound **4**.

2.3. FT-IR and NMR characterization

The neutral or anionic coordination of the benzoylhydrazone of this work was confirmed by infrared spectroscopy. The FT-IR spectra can be found in the supplemental material (Figs. S9-S12). The neutral coordination of HL in compound **1** is evident by the N—H stretching and bending vibration bands at 3214 and 1524 cm^{-1}, respectively, as well by the C═O stretching at 1637 cm^{-1} (1653 cm^{-1} in free HL (Fig. S8, [7,17]). In compounds **2, 3** and **4**, the C—O stretching band of $[L]^-$ appears at 1500, 1508 and 1505 cm^{-1}, respectively [7]. The C═N stretching bands of HL or $[L]^-$ appear at 1578 (for **1**), 1589/1557 (for **2**), 1584/1557 (for **3**), and 1584/1557 cm^{-1} (for **4**). Compared to the free ligand (1580 cm^{-1}), they shifted slightly to higher frequencies (~1585 cm^{-1} [7,25]) in compounds **2**–**4**. Two C═N bands were observed due to the formation of a new C═N bond from the deprotonation of the amide group in **2**–**4**.

In the spectrum of compound **1**, the nitrate stretching vibrations appear at 1415 and 1343 cm^{-1} [24]. The small Δν (72 cm^{-1}) confirms the chelate bidentate coordination mode [12]. In the spectrum of **2**, the bands at 1570 and 1336 cm^{-1} can be attributed to the asymmetric and symmetric stretching of the acetate ligand, respectively. The Δν (234 cm^{-1}) indicates the monodentate coordination of the acetate [26,27], which produces asymmetrical C—O(acetate) bonds in **2** (1.242(4) and 1.282(4) Å). In the spectrum of **4**, the asymmetric and symmetric stretching vibrations of the nitrite ligand appear at 1319 and 1154 cm^{-1} (Δν = 165 cm^{-1}), respectively [28,29]. Asymmetrical N—O bonds were observed in **4** [1.279(4) and 1.236(4) Å] and **1** [*e.g.* 1.275(3)/1.256(3)

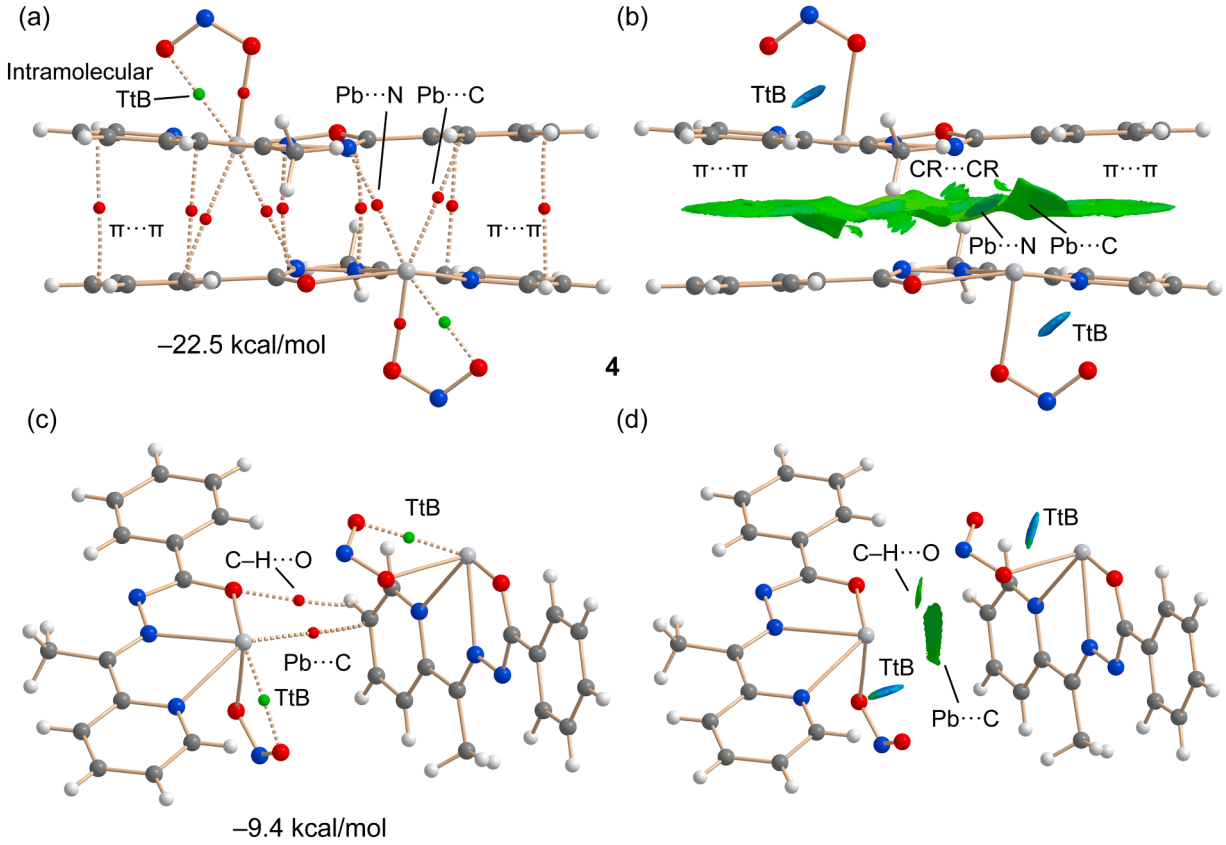

Fig. 11. (a,c) QTAIM analysis of the self-assembled dimers of **4** showing the bond critical points (BCPs) and bond paths (dashed lines) associated with the intermolecular (BCPs in red) and intramolecular (BCPs in green) interactions. (b,d) NCIplot analyses of the same dimers highlighting the π•••π and Pb•••η^2-C_2 interaction; light blue disks correspond to stronger non-covalent interactions (intramolecular tetrel bonds), while green surfaces indicate weaker interactions (π-stacking, CR•••CR, intermolecular Pb•••C and van der Waals forces).

and 1.232(3) Å].

The ^{1}H and ^{13}C NMR measurements were performed in DMSO-d_6 at 25 °C. HL and compounds **1** and **3** presented broad signals in the ^{1}H spectra. Therefore, measurements were performed at 60 °C for HL and **3**, giving spectra with better multiplicity resolution. For compound **3**, at 60 °C the solubility was increased, allowing measurement of a good ^{13}C spectrum as well. In case of compound **1**, heating was avoided since it could deprotonate the neutral ligand in the complex. Figs. S13-S19 contain the 1D and 2D spectra for HL.

For HL, the complete attribution of the signals in the ^{1}H and ^{13}C NMR spectra was possible from the spectra at 60 °C. The pyridyl carbon atoms appeared at 155.0, 148.3, 136.2, 123.7 and 120.1 ppm (60 °C). The signals of the hydrogen atoms from the pyridyl group in the ^{1}H spectrum were observed at 8.61 (doublet, $J = 4.3$ Hz), 8.04 (broad singlet), 7.83 (triplet, $J = 7.0$ Hz) and 7.40 (doublet of doublets, $J = 6.7$, 5.2 Hz). The NH signal was observed at 10.73 ppm (10.87 ppm at 25 °C and [17]). The signals of the carbonyl (C8) and azomethine (C6) carbon atoms were not detected at 60 °C, being seen in the spectrum recorded at 25 °C as small signals at 164.1 and 154.8 ppm, respectively.

The ^{1}H and ^{13}C spectra of compounds **1**–**4** are presented in Figs. S20-S33. Compounds **2** and **4** have well resolved signals in their ^{1}H spectra at 25 °C being also the 2D spectra measured (HSQC and HMBC). Coordination by deprotonation is clear by the shift of the signals of C6 and C8 carbon atoms (Table 3). Upon coordination, the azomethinic C6 atom shifts downfield from 154.8 ppm (HL) to 157.2 (in **2**) and 157.8 ppm (in **4**). The C8 carbon atom from the enolic tautomer shifts downfield at about 9 ppm in these two complexes. It, thus, corroborates with the crystal structures which contain the hydrazonate ligands. The formation of compound **3** is also confirmed by ^{13}C NMR with downfield shifts of C6 and C8 carbon atoms (Table 3).

In compound **1** ^{13}C NMR spectra, the coordination of HL as neutral ligand is evident by the similarity of the chemical shifts with free HL (Table 3). Coordination through the amide oxygen atom is inferred by the shift from 164.1 ppm (free HL) to 165.1 ppm (**1**). In the ^{1}H NMR, the spectrum characteristics is very similar to that of the ligand with broad signals recorded in the same solvent at 25 °C [30]. The amide NH signal shifts downfield from 10.87 ppm (HL) to 11.23 ppm (in **1**). Shifts are also seen for hydrogen atoms from pyridyl group. Most notably, H1 hydrogen atom shifts from 8.62 ppm (HL, Fig. S13) to 8.70 ppm (**1**, Fig. S20). As comparison, the H1 hydrogen atom signal in the ^{1}H spectra of compounds **2** and **4** are at 8.77 and 8.80 ppm as doublets ($J = 4.3$ Hz), respectively, and at 8.70 ppm for compound **3** (Fig. 12). Shift of the H7 hydrogen atoms (from methyl group) signal was also observed. Compared to the free ligand (2.47 ppm), in the Pb(II) complexes it appears at 2.53 (**1**), 2.68 (**2**), 2.66 (**3**) and 2.70 ppm (**4**) (Fig. S34). The presence of acetate as ligand in compound **2** was confirmed by the signals at 1.54 ppm (^{1}H NMR spectrum), and 26.3 and 177.0 ppm in the ^{13}C NMR spectrum (Fig. S24-S25).

Table 3
Selected ^{13}C NMR data for HL and compounds **1**–**4** (δ, ppm) in DMSO-d_6. The atoms numbering is shown in the ligand draw 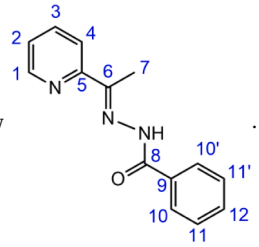 .

	HL (298 K)	HL (333 K)	**1** (298 K)	**2** (298 K)	**3** (333 K)	**4** (298 K)	Attribution
C1	148.3	148.6	148.7	148.5	148.4	148.4	*C*N(Py)
C5	155.0	155.1	155.6	152.2	153.9	152.2	*C*N(Py)
C6	154.8	154.8	154.2	157.2	156.4	157.8	*C*N(imine)
C8	–	164.1	165.1	173.3	172*	173.4	*C*O
C9	133.9	133.9	133.3	137.0	–	136.9	OCC(Ph)

* from HMBC spectrum. Py = pyridyl; Ph = phenyl.

2.4. *UV–Vis diffuse reflectance characterization*

The ligand of this work presents a phenyl and a pyridyl substituent on the sides of the –CO–NH–N=CH– sequence. It is well-known that upon deprotonation, the aryl substituents contribute in generating an extended π-conjugated system, stabilizing by resonance the hydrazone anion [1]. Compounds **2**–**4** contain a deprotonated hydrazonate ligand and are yellow colored. Compound **1** is white and reflects the coordination of the hydrazone ligand in its neutral form.

The diffuse reflectance measurements of compounds **1**–**4** were carried out in the wavelength range of 220–1000 nm. Fig. S35 depicts the diffuse reflectance spectra as a function of wavelength. Absorption spectra were obtained from reflectance values using the Kubelka-Munk function, $F(R) = (1-R)^2/2R$, where R is the reflectance [31]. Compound **1** absorbs only below 400 nm while compounds **2**–**4** also absorb in the visible region of the spectra (Fig. 13). The bands centered at 283 nm (for **1**), 324 nm (for **3**) and 338 nm (for **2** and **4**) correspond to intraligand π–π* transitions [12,32]. The bands which appear as shoulder from 400–450 nm justify the colored aspect of the solid samples of **2**–**4**.

3. Experimental

3.1. *Materials and apparatus*

Fourier transform infrared (FT-IR) spectra were measured on a Bruker VERTEX 70 spectrometer between 200 and 4000 cm^{-1} (resolution of 4 cm^{-1}) in the ATR mode. Elemental analysis of carbon, hydrogen, nitrogen and sulfur were determined using a PerkinElmer 2400 series II elemental analyzer. ^{1}H and ^{13}C NMR spectra were taken with a Bruker 600.13 MHz (for ^{1}H nuclei) AVANCE III spectrometer. The diffuse reflectance (DR) spectra of compounds **1** – **4** were recorded in a Shimadzu UV-2600 spectrophotometer equipped with a diffuse reflectance accessory (integrating sphere ISR 2600 Plus). Barium sulphate was used as white reference material. The DRS-UV–Vis spectra were calculated using the Kubelka-Munk treatment of the DR data [31].

Single-crystal diffraction data collection for compounds **1**–**4** and **3A** were obtained using a Bruker D8 VENTURE diffractometer with graphite monochromated Ag-Kα radiation (λ = 0.56086 Å) and a Photon 100 detector. The structures were solved using dual space method using Bruker XT and refined with Bruker XL on F^2 using anisotropic thermal parameters for all non-hydrogen atoms. The hydrogen atom positions were calculated starting from the geometric idealized positions. Data collection and structure refinement parameters, and the crystallographic data are given in Tables S1–S2. The anisotropic thermal ellipsoid plots of the compounds are in Figs. S1–S3. Additional information on the structure determination has been deposited with the Cambridge Crystallographic Data Centre (CCDC 2534816 – 2534820). These data can be obtained free of charge via www.ccdc.cam.ac.uk/structures.

3.2. *Syntheses*

2-Acetylpyridine benzoylhydrazone (HL ligand) was prepared by refluxing equivalent amounts (0.01 mol) of 2-acetylpyridine and benzoylhydrazine (benzhydrazide) in ethanol (20 mL) during 4 h [25]. The white solid formed on cooling the solution was filtered off. The solution was concentrated and more crystalline product was formed, which was filtered off and air-dried. Yield: 90%. Melting point: 154–155 °C. FT-IR (ATR, ν_{max} in cm^{-1}): 3178 [ν(NH)], 3004 [ν(CH)], 1653 [ν(C=O)], 1580 [ν(C=N)], 1541 [δ(CNH)], 1465 [ν(C=C)], 1430 [ν(C=C)], 1373, 1324, 1280 [δ(NNH)], 1137 [ν(N–N)], 781, 697 [δ(CCH)]. ^{1}H NMR (600.13 MHz, DMSO-d_6, 298 K): δ 10.87 (s, 1H, NH), 8.62 (s, 1H), 8.25–8.02 (m, 1H), 8.00–7.75 (m, 3H), 7.62–7.56 (m, 1H), 7.52 (t, J = 7.4 Hz, 2H), 7.42 (s, 1H), 2.47 (s, 3H, CH_3). ^{13}C NMR (150.90 MHz,

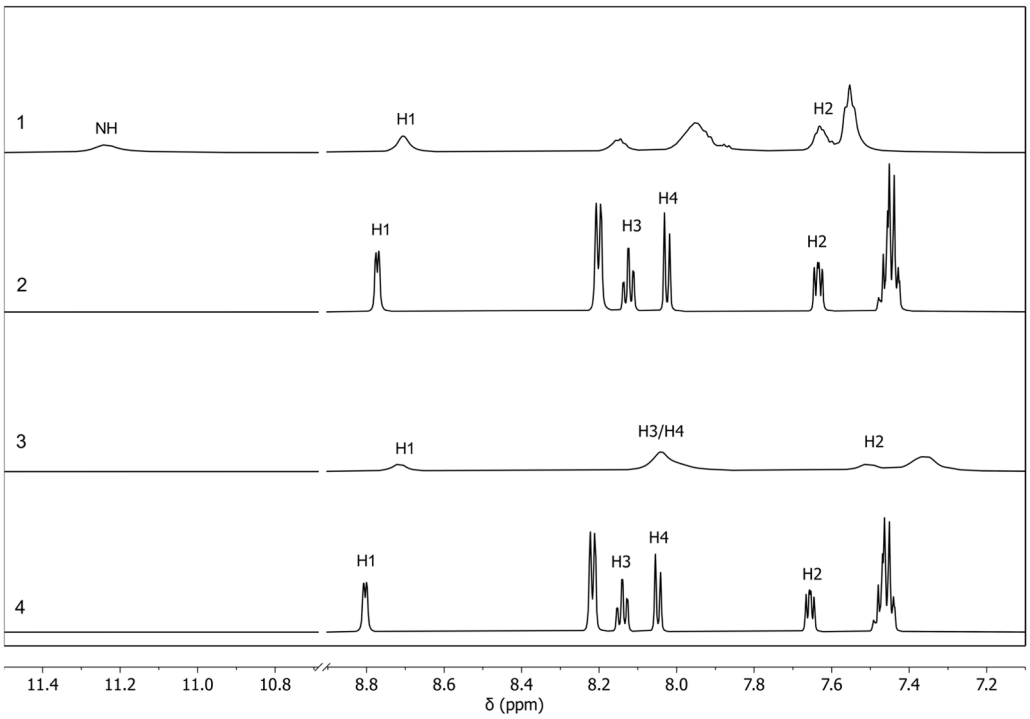

Fig. 12. The ^{1}H NMR spectra of the complexes recorded in DMSO-d_6 (25 °C). The H atoms signals from the pyridyl group(s) are labelled.

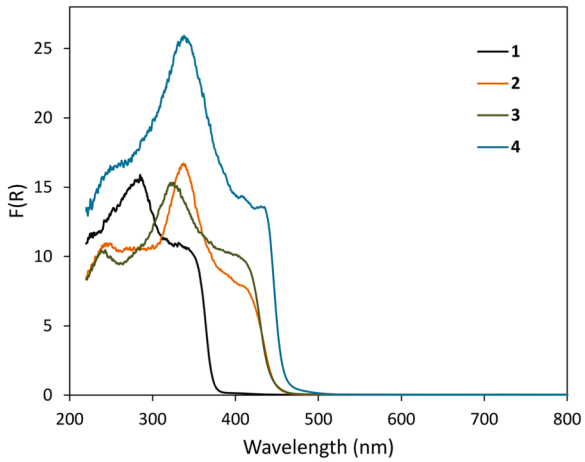

Fig. 13. Solid-state Kubelka-Munk absorbance spectra of compounds **1**–**4**.

DMSO-d_6, 298 K): δ 164.1 (C═O), 155.1, 154.8 (C═N), 148.6, 136.6, 133.9 (Ph), 131.6 (Ph), 128.3 (Ph), 128.0 (Ph), 124.1, 120.4, 12.6 (CH_3). ^{1}H NMR (600.13 MHz, DMSO-d_6, 333 K): δ 10.73 (s, 1H, NH), 8.61 (d, J = 4.3 Hz, 1H), 8.04 (s, 1H), 7.90 (d, J = 7.3 Hz, 2H), 7.83 (t, J = 7.0 Hz, 1H), 7.58 (t, J = 7.4 Hz, 1H), 7.52 (t, J = 7.5 Hz, 2H), 7.40 (dd, J = 6.7, 5.2 Hz, 1H), 2.47 (s, 3H, CH_3). ^{13}C NMR (150.90 MHz, DMSO-d_6, 333 K): δ 155.0, 148.3, 136.2, 133.9 (Ph), 131.1 (Ph), 128.0 (Ph), 127.9 (Ph), 123.7, 120.1, 12.2 (CH_3).

3.3. Synthesis of $[Pb(HL)_2(NO_3)_2]$ (1)

In a 50 mL flask, $Pb(NO_3)_2$ (33 mg, 0.10 mmol) was suspended in 4 mL of methanol. Then, solid HL (48 mg, 0.20 mmol) was added. The mixture was stirred for 2.5 h at room temperature and the white solid was filtered off and air-dried. Yield: 72% based on HL. Elemental Analysis: calc. for $C_{28}H_{26}N_8O_8Pb$: C, 41.53; H, 3.24; N, 13.84; found: C, 41.52; H, 3.22; N, 13.81. FT-IR (ATR, ν_{max} in cm^{-1}): 3214 [ν(NH)], 1637 [ν(C═O)], 1578 [ν(C═N)], 1524 [δ(CNH)], 1472 [ν(C═C)], 1415 [$\nu(NO)_{nitrate}$], 1343 [$\nu(NO)_{nitrate}$], 1275 [δ(NNH)], 1145, 784, 708. ^{1}H NMR (600.13 MHz, DMSO-d_6, 298 K): δ 11.23 (s, 1H), 8.70 (s, 1H), 8.36–8.06 (m, 1H), 8.06–7.71 (m, 3H), 7.69–7.59 (m, 1H), 7.59–7.43 (m, 3H), 2.53 (s, 3H). ^{13}C NMR (150.90 MHz, DMSO-d_6, 298 K): δ 165.1, 155.6, 154.2, 148.7, 137.5, 133.3, 132.1, 128.4, 128.2, 124.9, 121.7, 13.3.

Colorless plate-shaped crystals of **1** were obtained in the mother liquor within the slow evaporation of the solvent.

3.4. Synthesis of $[Pb(L)(CH_3CO_2)]_n$ (2)

In a 50 mL flask, $Pb(CH_3CO_2)_2{\bullet}3H_2O$ (38 mg, 0.10 mmol) was dissolved in 4 mL of methanol. Then, solid HL (24 mg, 0.10 mmol) was added. The mixture was stirred for 2 h at room temperature and the clear yellow solid was filtered off and air-dried. Yield: 65% based on HL. Elemental Analysis: calc. for $C_{16}H_{15}N_3O_3Pb$: C, 38.09; H, 3.00; N, 8.33; found: C, 39.81; H, 3.06; N, 8.71. FT-IR (ATR, ν_{max} in cm^{-1}): 1589 [ν(C═N)], 1570 [$\nu(C{-}O)_{acetate}$], 1557 [ν(C═N)], 1500 [ν(C—O)], 1464 [ν(C═C)], 1430 [ν(C═C)], 1360, 1336 [$\nu(C{-}O)_{acetate}$], 1151, 783, 705. ^{1}H NMR (600.13 MHz, DMSO-d_6, 298 K): δ 8.77 (d, J = 4.3 Hz, 1H), 8.19 (d, J = 6.6 Hz, 2H), 8.12 (td, J = 7.8, 1.6 Hz, 1H), 8.02 (d, J = 8.0 Hz, 1H), 7.63 (dd, J = 7.2, 5.1 Hz, 1H), 7.49–7.39 (m, 3H), 2.68 (s, 3H), 1.54 (s, 3H). ^{13}C NMR (150.90 MHz, DMSO-d_6, 298 K): δ 177.0, 173.3, 157.2, 152.2, 148.5, 139.7, 137.0, 130.2, 128.6, 128.1, 125.0, 123.6, 26.3, 14.3.

Yellow needles of **2** were formed in the filtrate by slow evaporation of the solvent for structural analysis.

Note: if 0.20 mmol of HL and N,N-dimethylformamide (3 mL, as solvent) were used, the yield is 63%.

3.5. Synthesis of $[Pb(L)_2]$ (3)

Method A: In a 50 mL flask, $Pb(CH_3CO_2)_2{\bullet}3H_2O$ (38 mg, 0.10 mmol) was dissolved in 4 mL of methanol. Then, solid HL (48 mg, 0.20 mmol) was added. To the resulting clear light yellow mixture, 4 drops of NEt_3 were added. Precipitation started in 2–3 min of stirring. Additional 2 mL

of methanol were added for better stirring of the mixture. After 2 h of stirring at room temperature, the clear yellow solid of **3** was filtered off and air-dried. Yield: 92% based on HL. Elemental Analysis: calc. for $C_{28}H_{24}N_6O_2Pb$: C, 49.19; H, 3.54; N, 12.29; found: C, 49.02; H, 3.41; N, 12.21. FT-IR (ATR, ν_{max} in cm^{-1}): 1584 [ν(C═N)], 1557 [ν(C═N)], 1508 [ν(C—O)], 1467 [ν(C═C)], 1434 [ν(C═C)], 1356, 1152, 783, 709. ^{1}H NMR (600.13 MHz, DMSO-d_6, 333 K): δ 8.68 (s, 1H), 8.20–7.74 (m, 4H), 7.45 (s, 1H), 7.40–7.14 (m, 3H), 2.65 (s, 3H). ^{13}C NMR (150.90 MHz, DMSO-d_6, 333 K): δ 156.4, 153.9, 148.4, 137.9, 129.2, 127.9, 127.4, 123.7, 122.4, 14.0.

Method B: In a 50 mL flask, $PbCO_3$ (53 mg, 0.20 mmol), HL (48 mg, 0.20 mmol) and 5 mL of *N,N*-dimethylformamide were added. The mixture was heated at 90–95 °C for 2.5 h under magnetic stirring. Then, the mixture was allowed to cool to room temperature and filtered using filter paper. The filtrate was collected in a flask for crystallization, and 2.5 mL of methanol were added. In ca. 2 days, yellow crystals of **3** (rectangular blocks/needles) and **3A** (blocks) were observed and collected for analysis. Yield: 75% based on HL.

Note: if methanol is not added, the crystallization takes longer.

3.6. Synthesis of [Pb(L)(NO$_2$)] (4)

In a 50 mL flask, $Pb(NO_3)_2$ (33 mg, 0.10 mmol) was suspended in 4 mL of methanol. Then, solid $NaNO_2$ (14 mg, 0.20 mmol) and HL (24 mg, 0.10 mmol) were added. The mixture was stirred for 2 h at room temperature and the yellow solid was filtered off and air-dried. Yield: 90% based on HL. Elemental Analysis: calc. for $C_{14}H_{12}N_4O_3Pb$: C, 34.21; H, 2.46; N, 11.40; found: C, 34.73; H, 2.34; N, 11.65. FT-IR (ATR, ν_{max} in cm^{-1}): 1584 [ν(C═N)], 1557 [ν(C═N)], 1505 [ν(C—O)], 1465 [ν(C═C)], 1435 [ν(C═C)], 1359, 1319 [$\nu(NO)_{nitrite}$], 1154 [$\nu(NO)_{nitrite}$], 777, 717. ^{1}H NMR (600.13 MHz, DMSO-d_6, 298 K): δ 8.80 (d, J = 4.3 Hz, 1H), 8.25–8.17 (m, 2H), 8.13 (td, J = 7.8, 1.5 Hz, 1H), 8.04 (d, J = 7.0 Hz, 1H), 7.65 (dd, J = 7.0, 5.2 Hz, 1H), 7.50–7.42 (m, 3H), 2.70 (s, 3H). ^{13}C NMR (150.90 MHz, DMSO-d_6, 298 K): δ 173.4, 157.8, 152.2, 148.4, 139.7, 136.9, 130.3, 128.5, 128.1, 125.0, 123.7, 14.4.

Yellow blocks of **4** were formed in the mother liquor when concentrated by slow evaporation of the solvent.

3.7. Theoretical methods

The geometry of the monomers and self-assembled dimers for complexes **3, 3A** and **4** were taken directly from their respective X-ray crystal structures without further optimization. This approach allows for the analysis of non-covalent interactions as they exist within the crystalline environment. Single-point energy calculations were carried out using Gaussian-16 [33] at the PBE0-D3/def2-TZVP level of theory [34–36]. The D3 version of Grimme's empirical dispersion correction with Becke-Johnson damping was applied to account for long-range van der Waals interactions [35], which are crucial for supramolecular assemblies. For the lead atom, the def2-TZVP basis set [36] was used in conjunction with the Stuttgart/Cologne effective core potential (ECP), which includes relativistic effects essential for the accurate description of heavy elements like Pb(II) [37].

The molecular electrostatic potential (MEP) surfaces were computed on the monomeric unit of **3** at an isosurface value of 0.001 a.u. The Quantum Theory of Atoms in Molecules (QTAIM) [38] and Non-Covalent Interaction (NCIplot) analyses [39] were performed on the single-point electron densities using the AIMAll software package [40]. Bond critical points (BCPs) and bond paths were located to characterize the nature of the Pb•••N and Pb•••C interactions. The NCIplot index, based on the reduced density gradient (RDG), was used to visualize and differentiate between various types of non-covalent interactions (steric clashes, van der Waals, and hydrogen/tetrel bonds) in real space.

The dimerization energies (ΔE) for the supramolecular assemblies observed in the crystal structures of **3** and **3A** were calculated as the difference between the energy of the optimized dimer and the sum of the energies of the isolated monomers: $\Delta E = E_{(dimer)} - 2E_{(monomer)}$. To account for the basis set superposition error (BSSE), which can be significant for weakly bound complexes, the counterpoise correction method of Boys and Bernardi was applied [41].

4. Conclusion

In this work, we have synthesized and characterized four new lead (II) coordination compounds with 2-acetylpyridine benzoylhydrazone (HL). The synthetic conditions, particularly the choice of counter-anion and the presence of a base, played a crucial role in the final stoichiometry and the protonation state of the ligand. Compound **1** crystallized with the neutral hydrazone ligand, exhibiting a holodirected geometry despite the presence of the inert pair effect. In contrast, deprotonation occurred in compounds **2**–**4**, leading to the formation of hydrazonate complexes with hemidirected geometries. Notably, compound **3** represents a rare example of a homoleptic Pb(II) complex with this class of ligands.

The analysis of the supramolecular architectures revealed that the crystal packing is governed by a complex interplay of non-covalent interactions. Experimental X-ray data suggested the presence of tetrel bonding interactions, specifically Pb•••O and Pb•••N contacts, in compounds **2** and **3**. A detailed DFT study, combining MEP, QTAIM, and NCIplot analyses, was performed to corroborate these observations and explore the energetics of the self-assembled dimers in compound **3** and its polymorph **3A**.

The theoretical results confirmed the existence of σ-holes on the lead (II) atoms, capable of interacting with electron-rich domains. In compound **3**, the calculations validated the presence of intermolecular Pb···N(azomethine) tetrel bonds. These, together with auxiliary C—H•••O hydrogen bonds and extensive van der Waals forces, result in a strongly bound dimer (–26.9 kcal/mol). In the case of polymorph **3A** and **4** the analysis unveiled a novel Pb•••η^2-C_2(arene) interaction, where the π-system of the phenyl or pyridyl ring acts as the electron donor. The identification of this interaction expands the understanding of the supramolecular landscape in lead(II) hydrazone complexes. Overall, this study highlights the significance of tetrel bonding and dispersive forces in directing the self-assembly of hemidirected lead(II) coordination polymers.

CRediT authorship contribution statement

Vânia Denise Schwade: Writing – review & editing, Writing – original draft, Methodology, Investigation, Formal analysis, Data curation, Conceptualization. **Luana Floriano:** Investigation, Formal analysis. **Antonio Frontera:** Writing – review & editing, Investigation, Funding acquisition. **Asmet N. Azizova:** Writing – review & editing, Software, Data curation. **Ghodrat Mahmoudi:** Visualization, Validation, Conceptualization.

Declaration of competing interest

The authors declare that they have no known competing financial interests or personal relationships that could have appeared to influence the work reported in this paper.

Acknowledgements

The authors gratefully acknowledge the financial support provided by the Brazilian funding agencies Conselho Nacional de Desenvolvimento Científico e Tecnológico (CNPq) (Grant process 141346/2010-8) and Coordenação de Aperfeiçoamento de Pessoal de Nível Superior (CAPES). The X-ray diffraction and the spectroscopy facilities were acquired with support from FINEP/CT-Infra.

Supplementary materials

Supplementary material associated with this article can be found, in the online version, at doi:10.1016/j.molstruc.2026.146840.

Data availability

Data will be made available on request.

References

[1] G. Antoniolli, G.R. de Moraes, C. Deruvo, C.D. Altomare, F. Coelho, M. de Candia, N-acylhydrazones: applications and advances in drug discovery, Eur. J. Med. Chem. Rep. 16 (2026) 100317, https://doi.org/10.1016/j.ejmcr.2025.100317.

[2] I. Kalikhman, B. Gostevskii, E. Kerstsnus, S. Deuerlein, D. Stalke, M. Botoshansky, D. Kost, Competing reactions of hypercocoordinate silicon dichelates, J. Phys. Org. Chem. 21 (2008) 1029–1034, https://doi.org/10.1002/poc.1391.

[3] I.I. Seifullina, N.V. Shmatkova, O.V. Shishkin, R.I. Zubatyuk, Germanium(IV) bischelates with 2-hydroxynaphthaldehyde pyridinoylhydrazones: the crystal and Molecular structure of the complex with isonicotinoylhydrazone (H_2Inf), [Ge(Inf·HCl)$_2$]·5H_2O, Russ. J. Inorg. Chem. 52 (4) (2007) 486–493, https://doi.org/10.1134/S0036023607040043.

[4] M.A. Affan, S.W. Foo, I. Jusoh, S. Hanapi, E.R.T. Tiekink, Synthesis, characterization and biological studies of organotin(IV) complexes with hydrazine ligand, Inorg. Chim. Acta 362 (14) (2009) 5031–5037, https://doi.org/10.1016/j.ica.2009.08.010.

[5] F.A. Afkhami, G. Mahmoudi, F. Qu, A. Gupta, E. Zangrando, A. Frontera, D. A. Safin, Supramolecular architecture constructed from the hemidirected lead(II) complexes with N'-(4-hydroxybenzylidene)isonicotinohydrazide, Inorg. Chim. Acta 502 (2020) 119350, https://doi.org/10.1016/j.ica.2019.119350.

[6] V.D. Schwade, E. Faoro, E.S. Lang, Intermolecular Pb···N interactions in lead(II) dimers producing a supramolecular two-dimensional metal–organic compound: bis[μ_2-*N*'-(2-oxidobenzylidene)benzohydrazidato-κ^4*O:o,N',O'*]dilead(II), ActaCryst 72 (2016) 525–529, https://doi.org/10.1107/S2053229616008755.

[7] V.D. Schwade, B. Tirloni, R.A. Burrow, E.S. Lang, Lead(II) thiocyanate reaction behaviour with hydrazones, Polyhedron. 188 (2020) 114707, https://doi.org/10.1016/j.poly.2020.114707.

[8] L. Shimoni-Livny, J.P. Glusker, C.W. Bock, Lone pair functionality in divalent lead compounds, Inorg. Chem. 37 (8) (1998) 1853–1867, https://doi.org/10.1021/ic970909r.

[9] A. Bauzá, S.K. Seth, A. Frontera, Tetrel bonding interactions at work: impact on tin and lead coordination compounds, Coord. Chem. Rev. 384 (2019) 107–125, https://doi.org/10.1016/j.ccr.2019.01.003.

[10] J.-H. Chung, B.-K. Min, Y.K. Kim, K.-H. Kim, T.-Y. Kwon, From discrete to infinite 3D coordination polymer: sonochemical syntheses and structural characterization of a new nano flower lead (II) coordination compound, J. Mol. Struct. 1076 (2014) 698–703, https://doi.org/10.1016/j.molstruc.2014.08.019.

[11] M.K. Hema, I. García-Santos, A. Castiñeras, M. Mehrabian, E. Zangrando, R. J. Ramalingam, B.N. Ramakrishna, N.K. Lokanath, C.S. Karthik, G. Mahmoudi, Cg…Cg interactions driven 1D polymeric chains bridged by lattice solvents in N^3-(2-pyridoyl)-4-pyridinecarboxamidrazone Pb(II) complex, J. Mol. Struct. 1294 (2023) 136420, https://doi.org/10.1016/j.molstruc.2023.136420.

[12] V.O. Araujo, G.A. Casagrande, B. Tirloni, V.D. Schwade, Lead(II) compounds with neutral coordination of semicarbazones: synthesis and characterization, Inorg. Chim. Acta 533 (2022) 120785, https://doi.org/10.1016/j.ica.2021.120785.

[13] Y.A. Tyula, A. Zabardasti, H. Goudarziafshar, B. Mirtamizdoust, A new hemidirected lead(II) complex extended in holodirected one-dimensional polymer by secondary Pb−O interactions: a precursor for preparation of PbO nanoparticles, and DFT study, J. Mol. Struct. 1149 (2017) 142–148, https://doi.org/10.1016/j.molstruc.2017.07.090.

[14] S.A. Southern, D. Errulat, J.M. Frost, B. Gabidullin, D.L. Bryce, Prospects for ^{207}Pb solid-state NMR studies of lead tetrel bonds, Faraday Discuss. 203 (2017) 165–186, https://doi.org/10.1039/c7fd00087a.

[15] C. Gourlaouen, J.-P. Piquemal, On the quantum chemical nature of lead(II) "Lone pair, Molecules. 27 (2022) 27, https://doi.org/10.3390/molecules27010027.

[16] J. Masternak, B. Barszcz, M. Hodorowicz, O.V. Khavryuchenko, A. Majka, Synthesis and physicochemical characterization of two lead(II) complexes with O-, N-donor ligands. Lone pair functionality and crystal structure, Spectrochim. Acta Part A 136 (2015) 1998–2007, https://doi.org/10.1016/j.saa.2014.07.084.

[17] J. Patole, U. Sandbhor, S. Padhye, D.D. Deobagkar, C.E. Anson, A. Powell, Structural chemistry and In vitro antitubercular activity of acetylpyridine benzoyl hydrazone and its copper complex against *mycobacterium smegmatis*, Bioorg. Med. Chem. Lett. 13 (2003) 51–55, https://doi.org/10.1016/S0960-894X(02)00855-7.

[18] D.-Q. Li, X. Liu, J. Zhou, Two new hemidirected lead(II) complexes: [Pb(pcih)(bha)] and [Pb(pcih)(NO3)], Z. Naturforsch 65 (2010) 1084–1088, https://doi.org/10.1515/znb-2010-0905.

[19] B. Mirtamizdoust, D.C. Bieńko, Y. Hanifehpour, E.R.T. Tiekink, V.T. Yilmaz, P. Talemi, S.W. Joo, Preparation of a novel nano-scale lead (II) zig-zag metal–Organic coordination polymer with ultrasonic assistance: synthesis, crystal structure, thermal properties, and NBO analysis of [Pb(μ-2-pinh)N3 H2O]n, J. Inorg. Organomet. Polym 26 (2016) 819–828, https://doi.org/10.1007/s10904-016-0385-8.

[20] S.S. Batsanov, Van der Waals radii of the elements, Inorg. Mater. 37 (2001) 871–885, https://doi.org/10.1023/A:1011625728803.

[21] G. Mahmoudi, S.K. Seth, A. Bauzá, F.I. Zubkov, A.V. Gurbanov, J. White, B. Stilinović, T. Doert, A. Frontera, Pb···X (X = N, S, I) tetrel bonding interactions in Pb(II) complexes: x-ray characterization, Hirshfeld surfaces and DFT calculations, CrystEngComm. 20 (2018) 2812–2821, https://doi.org/10.1039/C8CE00110C.

[22] G. Mahmoudi, A. Bauzá, M. Amini, E. Molins, J.T. Mague, A. Frontera, On the importance of tetrel bonding interactions in lead(II) complexes with (iso) nicotinohydrazide based ligands and several anions, Dalton. Trans. 45 (2016) 10708–10716, https://doi.org/10.1039/C6DT01947A.

[23] G. Mahmoudi, M. Abedi, S.E. Lawrence, E. Zangrando, M.G. Babashkina, A. Klein, A. Frontera, D.A. Safin, Tetrel bonding and other non-covalent interactions assisted supramolecular aggregation in a new Pb(II) complex of an isonicotinohydrazide, Molecules 25 (2020) 4056, https://doi.org/10.3390/molecules25184056.

[24] M.T. Weller, N.A. Young, Vibrational Spectroscopy [In: Characterisation Methods in Inorganic Chemistry], Oxford University Press, 2017.

[25] C.C. Gatto, E.S. Lang, A. Kupfer, A. Hagenbach, D. Wille, U. Abram, Dioxouranium complexes with acetylpyridine benzoylhydrazones and related ligands, Z. Anorg. Allg. Chem. 630 (2004) 735–741, https://doi.org/10.1002/zaac.200400024.

[26] G. Mahmoudi, I. Garcia-Santos, A. Castiñeiras, A.V. Gurbanov, Ö.F. Tutar, E. V. Panova, R.M. Gomila, A. Frontera, D.A. Safin, Tetrel bonding stabilized supramolecular dimer versus coordination polymer, obtained from N'-benzoylpyrazine-2-carbohydrazonamide and lead(II) acetate, J. Mol. Struct. 1365 (2026) 145920, https://doi.org/10.1016/j.molstruc.2026.145920.

[27] K. Nakamoto, Applications in Coordination Chemistry [In: Infrared and Raman Spectra of Inorganic and Coordination Chemistry – Part B], John Wiley & Sons, Inc, 1997, 5th Ed.

[28] Y. Hanifehpour, T. Zhou, B. Mirtamizdoust, H. Mostaanzadeh, S.W. Joo, Ultrasound-assisted synthesis of a novel nano-zigzag-pattern lead (II) metal–Organic system: a new precursor to produce nano-sized PbO, J. Inorg. Organomet. Polym. 27 (2017) 552–561, https://doi.org/10.1007/s10904-017-0497-9.

[29] M.A. Hitchman, G.L. Rowbottom, Transition metal nitrite complexes, Coord. Chem. Rev. 42 (1) (1982) 55–132, https://doi.org/10.1016/S0010-8545(00)80527-5.

[30] G. Mahmoudi, I. Garcia-Santos, A. Castiñeiras, A.V. Gurbanov, Ö.F. Tutar, E. V. Panova, R.M. Gomila, A. Frontera, D.A. Safin, Supramolecular coordination polymers, obtained from multidentate *N'*-benzoylpyrazine-2-carbohydrazonamide and a variety of salts PbX_2 (X = Cl^-, NO_3^-, NO_2^-, SCN^-), derived from tetrel and other noncovalent bonds, Inorg. Chem. Commun. 185 (2026) 116058, https://doi.org/10.1016/j.inoche.2025.116058.

[31] S. Nilavazhagan, D. Anbuselvan, A. Santhanam, N. Chidhambaram, Effect of an alkali hydroxide concentration on the structural, optical, and surface morphological properties of ZnO nanoparticles, Appl. Phys. A 126 (4) (2020) 279, https://doi.org/10.1007/s00339-020-3462-3.

[32] V.D. Schwade, V.O. Araujo, A. Lunardi, A.C. Micheletti, G.G. Rossi, M.M.A. de Campos, B. Tirloni, Easy obtention of tin(II) complexes by using semicarbazones in their hydrochloride forms, J. Mol. Struct. 1295 (2024) 136699, https://doi.org/10.1016/j.molstruc.2023.136699.

[33] Gaussian 16, Revision C.01, M.J. Frisch, G.W. Trucks, H.B. Schlegel, G.E. Scuseria, M.A. Robb, J.R. Cheeseman, G. Scalmani, V. Barone, G.A. Petersson, H. Nakatsuji, X.Li, M. Caricato, A.V. Marenich, J. Bloino, B.G. Janesko, R. Gomperts, B. Mennucci, H.P. Hratchian, J.V. Ortiz, A.F. Izmaylov, J.L. Sonnenberg, D. Williams-Young, F. Ding, F. Lipparini, F. Egidi, J. Goings, B. Peng, A. Petrone, T. Henderson, D. Ranasinghe, V.G. Zakrzewski, J. Gao, N. Rega, G. Zheng, W. Liang, M. Hada, M. Ehara, K. Toyota, R. Fukuda, J. Hasegawa, M. Ishida, T. Nakajima, Y. Honda, O. Kitao, H. Nakai, T. Vreven, K. Throssell, J.A. Montgomery Jr. J.E. Peralta, F. Ogliaro, M.J. Bearpark, J.J. Heyd, E.N. Brothers, K.N. Kudin, V.N. Staroverov, T.A. Keith, R. Kobayashi, J. Normand, K. Raghavachari, A.P. Rendell, J.C. Burant, S.S. Iyengar, J. Tomasi, M. Cossi, J.M. Millam, M. Klene, C. Adamo, R. Cammi, J.W. Ochterski, R.L. Martin, K. Morokuma, O. Farkas, J.B. Foresman, D.J. Fox, Gaussian, Inc., Wallingford CT, 2016.

[34] C. Adamo, V. Barone, Toward reliable density functional methods without adjustable parameters: the PBE0 model, J. Chem. Phys. 110 (13) (1999) 6158–6170, https://doi.org/10.1063/1.478522.

[35] S. Grimme, S. Ehrlich, L. Goerigk, Effect of the damping function in dispersion corrected density functional theory, J. Comput. Chem. 32 (7) (2011) 1456–1465, https://doi.org/10.1002/jcc.21759.

[36] F. Weigend, R. Ahlrichs, Balanced basis sets of split valence, triple zeta valence and quadruple zeta valence quality for H to Rn: design and assessment of accuracy, Phys. Chem. Chem. Phys. 7 (18) (2005) 3297, https://doi.org/10.1039/B508541A.

[37] D. Andrae, U. Häußermann, M. Dolg, H. Stoll, H. Preuß, Energy-adjusted ab initio pseudopotentials for the second and third row transition elements, Theor. Chim. Acta 77 (1990) 123–141, https://doi.org/10.1007/BF01114537.

[38] R.F.W. Bader, Atoms in Molecules: A Quantum Theory, Oxford University Press, Oxford, 1990.

[39] J. Contreras-García, E.R. Johnson, S. Keinan, R. Chaudret, J.-P. Piquemal, D. N. Beratan, W. Yang, NCIPLOT: a program for plotting noncovalent interaction regions, J. Chem. Theory. Comput. 7 (3) (2011) 625–632, https://doi.org/10.1021/ct100641a.

[40] T.A. Kith, AIMAll (Version 19.10.12); TK Gristmill Software: Overland Park, KS (2019). http://aim.tkgristmill.com.

[41] S.F. Boys, F. Bernardi, The calculation of small molecular interactions by the differences of separate total energies. Some procedures with reduced errors, Mol. Phys. 19 (4) (1970) 553–566, https://doi.org/10.1080/00268977000101561.